Available online at www.sciencedirect.com

ScienceDirect

Proceedings of the Combustion Institute 37 (2019) 2801–2808

Proceedings of the Combustion Institute

www.elsevier.com/locate/proci

Molecular-beam mass spectrometry study of oxy-combustion in a novel coal-plate experiment

Daniel Felsmann*, Martina Baroncelli, Joachim Beeckmann, Heinz Pitsch

Institute for Combustion Technology, RWTH Aachen University, Templergraben 64, Aachen 52062, Germany

Received 29 November 2017; accepted 2 July 2018
Available online 3 October 2018

Abstract

Oxy-fuel coal combustion could play a significant role in the foreseeable future for its application in carbon capture and storage (CSS) technologies. Therefore, detailed knowledge about the ongoing chemical kinetics in the combustion process is necessary. Here, we present an explorative approach to study volatile species gas phase kinetics in a novel coal-plate experiment probed with molecular-beam mass spectrometry. This coupling allows for time-resolved quantitative measurements of the gas-phase directly above the surface of solid fuels, which aid gaining more insight into the gas phase chemistry during coal combustion by detailed speciation information. Two coal samples, a rhenish lignite and a coal manufactured from hydrothermal carbonization, were chosen for this investigation due to their similar classification but different molecular structures. For both samples, our measurements show a two-stage devolatilization phase separated by a char-oxidation phase which can be attributed to the interaction of oxygen consumption in the gas phase and on the surface and the release of volatiles from deeper layers of the plate. Furthermore, detailed speciation data of light, oxygenated, and tar species allowed to identify fuel structure-specific decomposition patterns of the two different coal materials, thus providing comprehensive data that can be used for future model validation purposes.

Keywords: Coal combustion; Molecular-beam mass spectrometry; Chemical kinetics; Oxy-fuel

1. Introduction

Despite the increasing contribution of renewables supplying the energy demand, coal combustion will still play a major role in the foreseeable future [1]. Among fossil fuels, coal is the most carbon dioxide intensive energy resource and significant efforts are currently undertaken to reduce its environmental impact. For reaching this goal, carbon capture technologies, such as oxy-fuel combustion, have a cruicial role, as already pointed out in the Paris agreement of 2016 [2]. In oxy-fuel combustion, O_2 rather than air is used as oxidizer, which is then usually diluted with the flue-gas CO_2 to keep the temperature similar to air combustion. The development of large-scale oxy-fuel facilities requires a detailed knowledge of the combustion process under this unconventional atmosphere. Coal combustion is a complex

* Corresponding author.
E-mail address: d.felsmann@itv.rwth-aachen.de (D. Felsmann).

https://doi.org/10.1016/j.proci.2018.07.003
1540-7489

multiphase process characterized by three main steps: devolatilization, gas-phase combustion, and char burnout [3]. Tar and lighter gases are formed within these phases, and their yield and composition depends on parameters such as temperature, heating rate, and pressure. Competing effects for volatile release from the solid like bond breaking, cross-linking, and mass transport are sensitive to temperature. Hence, at high heating rates (10^4K/s) the ceiling yield is increased by up to 11% and the average mass of released volatile matter shifts from ∼150 amu at low heating rates (1 K/s) to ∼400 amu [4,5]. To this end, different experimental approaches and facilities were used and detailed critical reviews of these experiments can be found in Solomon et al. [6] and Haustein et al. [7]. Entrained flow reactors, drop tubes, and heated grids were utilized to investigate the devolatilization and sometimes also the oxidation process at high heating rates. These facilities aim at reproducing the furnace environment with the disadvantages that particle temperature histories and secondary reactions are not perfectly controlled. On the other hand, low heating rate experiments like thermogravimetric analysis are less representative of furnace conditions, but allow for a better control of the experimental conditions. In these experiments, gas analysis can be performed with different techniques, such as FTIR spectroscopy or gas chromatography [6,8], which allowed to identify several light volatiles and global amounts of tar. Molecular-beam mass spectrometry offers the opportunity to identify a large number of species in a short time and was applied by Dayton et al. [9] to investigate alkali production in biomass combustion, but without quantification of the signals.

In the present study, a burner stabilized stagnation flame setup was developed to investigate the gas-phase kinetics of different coals. The applied low heating rates lead to expression of volatile species with masses up to ∼180 amu while the experimental configuration allows for time- and space-resolved quantitative species and temperature measurements. Compared with most coal particle combustion experiments, the plate setup has several advantages. It provides an environment where inhomogeneous states like transport phenomena through the solid occur within controlled conditions. Detailed species analysis then enables to draw conclusions to coal type specific gas-phase kinetics from different combustion states. Furthermore, it can be well adapted to 1D numerical codes, like the one of Gentile et al. [10] which includes transport phenomena as well as chemical kinetics, to allow for detailed chemistry studies and model development, here already supported by a dataset for a well characterized lignite-like synthetic coal made from cellulose. On the other hand, the setup requires some compromises. First, the heating rates achieved in this experiment are relatively low. While these can be substantially increased above the values discussed below, they will remain lower than in typical pulverized coal applications. Secondly, the thickness of the coal plate used here is relatively large, but it was chosen to allow for testing the coupling of transport processes inside and outside the solid in a well controlled experiment. Third, the gas stream has a large fraction of Ar, which is needed for a reliable quantification of emitted species.

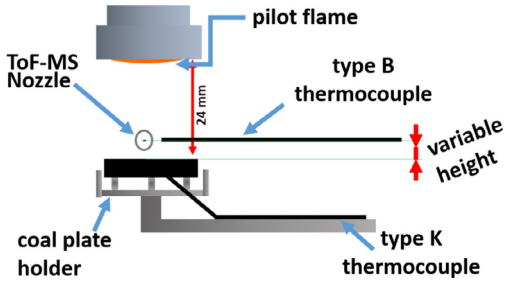

Fig. 1. Schematic drawing of the experimental setup.

2. Experiments

2.1. Experimental system

Analysis of the gas-phase coal combustion was performed with a setup consisting of a premixed flame burner and a coal plate in a stagnation point flow configuration. Niioka and Visser used this type of setup in the 1980s to characterize the ignition and combustion of solid propellants and graphite [11,12]. This experiment enables an investigation of the gas-phase combustion above solid fuels, while still maintaining a configuration that can be described by one-dimensional simulations. Figure 1 depicts a schematic drawing of the setup, basically consisting of a solid-fuel plate and a premixed laminar burner that delivers a hot gas stream. The simplicity of this setup allows the application of selected techniques to perform time-resolved measurements of species, temperature and optical phenomena connected to different combustion regimes. Powder of solid fuel is pressed to form a plate and is mounted on a horizontally movable holder that allows a fast introduction into the hot exhaust gas stream of a laminar premixed flame stabilized on a top-mounted pilot burner. The pilot flame provides relatively high gas temperatures not easily reachable by electric heating and a broad field of tunable parameters like temperature, strain, and gas composition through variation of stoichiometry, total flow and fuel. Videos are recorded with a Canon EOS 1200D at 25 frames/second while temperature histories are tracked by 1 mm sheathed thermocouples, with one touching the the bottom of the plate (T_{below}, K-type) and the other mounted at the same height above the coal

Table 1
Proximate and ultimate analysis of the two coals (water free) in wt% along with density ρ, effective surface in gas stream α, and average pore diameter Φ of the coal plates. The amount of oxygen was calculated by $O(wt\%) = 100 - Ash(wt\%) - C(wt\%) - H(wt\%) - N(wt\%) - S(wt\%)$.

	Vol/wt%	Ash/wt%	C/wt%	H/wt%	N/wt%	S/wt%	O/wt%	$\rho/\frac{g}{cm^3}$	$\alpha/\frac{m^2}{g}$	Φ/nm
HTC	53.0	0	65.0	4.2	–	–	30.8	0.90	3.229	2.1
RL	49.1	5.8	64.9	4.5	1.2	0.3	23.3	1.17	0.078	2.4

than the sampling nozzle (T_{above}, B-type). For speciation measurements along the centerline, electron-ionization time-of-flight molecular-beam mass spectrometry (EI-ToF-MBMS) was applied. EI-ToF-MBMS is a well-established technique for quantitative in-situ species analysis in systems such as laminar premixed low-pressure flames or flow reactors [13,14]. In brief, a gas probe is sampled out of the combustion process and expanded into a high vacuum to form a molecular beam in which reactions are frozen. This molecular beam is further focused through a skimmer into an ionization chamber where the sampled molecules are ionized. The ionized molecules are finally separated and detected by a time-of-flight mass spectrometer, which allows identification of species based on their CHO-composition derived from the ions mass-to-charge (m/z) ratio. Separation of hydrocarbons and oxygenated species up to m/z = 200 is thus achieved by reflectron time-of-flight with a mass resolution of $m/\Delta m \approx 4000$. A repetition frequency of about 35 kHz allows to operate in time-resolved mode for tracking unsteady processes like combustion of a coal plate in stagnation point flow. Another feature arises from the systems ability to be moved in vertical direction, allowing sampling at different heights above the plate adding a spatial dimension to the already time-resolved measurements. More technical detail of the instrument is provided in the supplemental material.

2.2. Coal characterization and preparation

Two different solid fuels, rhenish lignite (RL) from RWE Frechen and a lignite-like fuel obtained by hydrothermal carbonization of cellulose (HTC) [15], were investigated in this study. While RL represents a commonly used lignite coal, the HTC was chosen as a reference coal due to its well-defined and reproducible composition and structural stability. Proximate and ultimate analysis, shown in Table 1, demonstrate that the H/C and O/C ratio of both samples are very similar, only slight differences arise due to the RL containing ash as well as small amounts of N and S components. Both fuels were delivered as powder and were used without any pre-treatment for manufacturing coal plates used as analytes. Each plate was manufactured from 6.0 g of the sample and pressed at 25 t for 30 s in a hydraulic press. The final plates possess a diameter of 36 mm with thicknesses of 5.0 mm for RL and 6.5 mm for HTC samples, respectively.

Table 2
Exhaust composition of gas stream produced by the lean premixed methane pilot flame with and without argon taken into account.

	Ar	H_2O	O_2	CO_2	CO
x_i - w Ar	74.9	13.7	4.6	6.5	0.3
x_i - w/o Ar	–	54.6	18.3	25.9	1.2

2.3. Experimental procedure and conditions

An argon-diluted lean methane pilot flame (ϕ = 0.75, mol% of 7% CH_4 / 18% O_2 / 75% Ar, $T_{adiabatic} = 2250K$ [16]) with a total cold gas flow of 27.44 standard liter per minute was chosen to investigate the solid fuel combustion under oxy-fuel conditions. Gases were metered by calibrated mass flow controllers with errors less than 2%. Exhaust equilibrium concentrations, given in Table 2, were calculated with GasEQ [16] and recombination of OH and H radicals at the sampling nozzle has been taken into account by adding their respective mole fractions to the mole fraction of H_2O. The pilot flame conditions were chosen as a compromise between argon as a mandatory inert reference species for quantification of the signals and the hot reaction gas composition beeing close to oxy-fuel conditions (see Table 2). Plates were placed 24 mm away from the burner exit to prevent air entrainment in the sampling zone while assuring the desired equilibrium concentrations to be fully reached in the hot gas stream. The quartz nozzle for gas sampling was positioned at the centerline and a given distance relative to the plate surface. Before moving the plate into the gas stream, two background measurements were recorded and a nominal energy of ionizing electrons of 21 eV was used for ionization. An accumulation time of 15 s for each measurement point was necessary to achieve a signal-to-noise ratio sufficient for quantification of low concentration volatile species. The chosen energy was high enough to assure the ionization of all species including argon and low enough to induce only slight fragmentation of low ionizing species. Measurements are performed at 2, 3, 4, 5 mm above the plate surface to additionally track the species development in spatial direction. For each height,

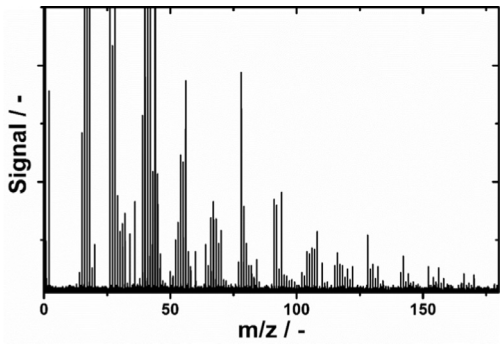

Fig. 2. Mass spectrum obtained from a 15 s averaged sample at 2 mm above the RL plate at a time corresponding to the maximum volatile output.

a separate coal plate had to be used, since these are consumed within one combustion process. Here, a test with six plates at one height revealed that the overall repeatability of the measurements is within 40%, which most likely is caused by the plate manufacturing process. An example of a mass spectrum from the gas phase above the coal is depicted in Fig. 2. This spectrum was recorded 2 mm above the RL at 195 s. With the accumulation time of 15 s, as many as 49 species with a m/z up to 178 and mole fractions as low as 10^{-6} were quantified, delivering a time-resolved comprehensive dataset of species in the gas phase above different coal plates.

2.4. Data evaluation

Data evaluation follows the procedures for quantitative MBMS measurements of laminar premixed low-pressure flames described extensively in the literature [17,18]. Major species ($x_i \geq 0.02$) can be calibrated based on the CHO elemental balance from the initial gas composition. Here, the assumption was made that Ar, CO_2, H_2O, CO, and O_2, account to more than 98% of the probe composition and that it is reasonable to define the exhaust equilibrium concentration of these species as inlet parameter for the quantification process. The errors for these mole fractions are estimated to be less than 15%. Quantification of intermediate species i follows a calibration procedure using a calibration factor $k_{i/R}(E)$ that includes all machine and energy-dependent variables of the species i relatively to a species R [17]. Reference species R in this study is the diluent gas argon and the calibration factors for all intermediate species were then generated from a convolution of literature ionization cross sections with known kinetic energy distribution of the ionizing electrons [17]. Hence, due to the nature of the calibration method, the uncertainties of all intermediate species mole fractions add up to a factor of 2. Additionally, the data for T_{above} was corrected for radiation losses occurring at these high temperatures. The correction was performed following the approach by Shaddix [19] and accounts for up to 450 K with an absolute uncertainty of up to ± 130 K. For better readability, error bars are not shown in the temperature curves of T_{above} in Figs. 4 and 5, but are shown in the supplementary material in Fig. S2.

3. Results

The results are organized in two sections. The first focuses on the global combustion process of the HTC synthetic coal that can be deduced from major species, temperature profiles, and optical observations. The second shows a comparison of different coal samples based on the quantitative MBMS measurements.

3.1. Global combustion process

Generally, it is observed in our measurement that both investigated coal samples show similar stages of combustion. Therefore, the observed and deduced effects are discussed for the HTC, while data for the RL can be found in the supplemental material (Figs. S3 and 4). The differences are discussed in more detail in Section 3.2.

Coal combustion is a multi-phase process and typically follows three basic phases: (i) Coal heat-up and drying; (ii) devolatilization, homogeneous ignition, and gas-phase combustion of volatiles; (iii) heterogeneous ignition and char oxidation. Observations of these phases for the coal plate are shown in Fig. 3. After insertion of the coal, a slight blueish glow attached to the coal surface is indicating water evaporation and start of devolatilization (Fig. 3a). Homogeneous ignition is seen in the form of a rapidly appearing yellow flame with a bright luminescent effect in its core above the coal plate (Fig. 3b).

During that time, the combustion of volatiles in a diffusion flame consumes all oxygen and heterogeneous char oxidation cannot happen. Subsequently, the brightness of the luminescent core diminishes, until at 55 s (Fig. 3c) a weaker yellow diffusive flame with a height of around 5 mm is observed. At 150 s (Fig. 3d), a strongly glowing coal surface indicates that the devolatilization rate has decreased so much that oxygen reaches the surface leading to the initiation of char oxidation, which is typically the final phase of coal combustion. Here, however the intensity of the gas flame above the coal increases again at 200 s for a short time of about 60 s showing a maximum at 225 s (Fig. 3e) before the optically visible gas-phase combustion terminates and only heterogeneous combustion occurs (Fig. 3f). Such two-stage behavior has so far only been observed in thermogravimetric measurements with low heating rates and oxidizing conditions [20,21]. This effect occured already at

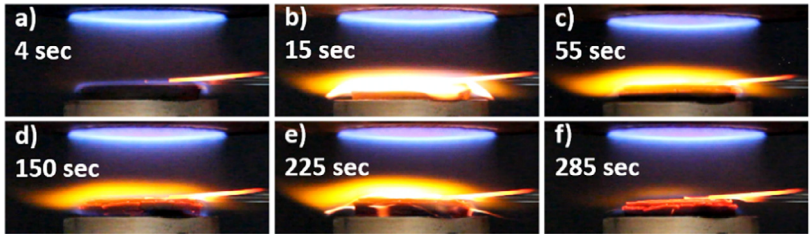

Fig. 3. Different stages of the HTC plate combustion process. a: Water evaporation; b: Start of devolatilization and homogeneous ignition; c: First maximum measured in CO; d: After first devolatilization stage with clearly visible heterogeneous ignition; e: Second devolatilization maximum; f: Steady state char burning after complete devolatilization.

particles with a size as small as 350–500 μm and was traced back to hetero-homogeneous ignition [20], but was not further explained. Here, the species and temperature data discussed in the following enable a closer evaluation. Measured time histories of mole fractions of O_2, CO_2, CO, and H_2O are shown in Fig. 4, as well as temperatures at the sampling position above and below the plate for altered positions from 2–5 mm above the surface. Once the coal is inserted at 0 s, O_2 is rapidly consumed and the concentrations of H_2O, CO_2, and CO rise at all sampling heights. The start of water evaporation before devolatilization could not be tracked sufficiently with the MBMS for HTC, because it happens on a time scale faster than the signal accumulation time of 15 s. Still, for low sampling heights, it is visible as a temperature drop (T_{above}, Fig. 4 upper panel) after insertion of the plate. The subsequent local temperature maximum at 15 s can be interpreted as homogeneous ignition of the volatiles, represented here by a strong rise in CO mole fraction, which reaches 19% at 2 mm within the first phase, while CO_2 and H_2O mole fractions stay roughly constant. This first devolatilization occurs due to heating of the surface from energy released by the hot gas and combustion of the volatiles. The spread of the volatile combustion zone in the gas-phase can be tracked with the height-dependent temperature histories measured (Fig. 4 upper panel). Close to the surface at 2 mm, the influence of the heat transfer to the surface of the plate is visible by a reduced temperature, while already at 3 mm sampling height, the share of heat transfer is significantly reduced and only water evaporation at 5 s is clearly visible through a drop in temperature. An increase of temperature is observed at both devolatilization peaks for 4 and 5 mm measurements showing that combustion of the volatile species dominates at these heights. Hence, in this first phase, linear extrapolation of the temperatures measured at 2–4 mm above the plate reveals a rate of 66 K/min, while the temperature at the bottom of the plate increases by 48 K/min, showing a slow heat-up of the plate through the energy from the gas stream

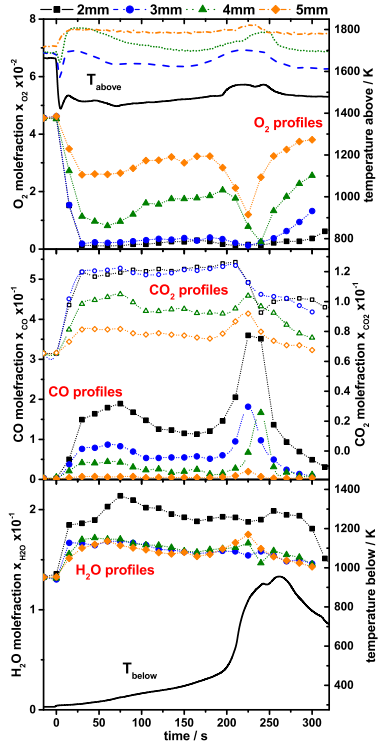

Fig. 4. Upper temperature profiles (lines) along with mole fraction profiles of O_2 (symbols, upper panel), CO_2 (open symbols) and CO (symbols, middle panel), and bottom temperature profile (line) as well as H_2O profiles (symbols, lower panel) for different sampling positions (2, 3, 4, and 5 mm) above the HTC. Lines in the experimental data shall guide the eye and do not reflect the measurement points.

and the volatile combustion. Oxygen is rapidly consumed by the released volatiles within the first 30 s. The measurements also show that at this time, O_2 is fully consumed at 2 and 3 mm, which implies that no oxygen reaches the surface of the plate. Therefore, combustion and volatile release is slowed down and char ignition is hindered.

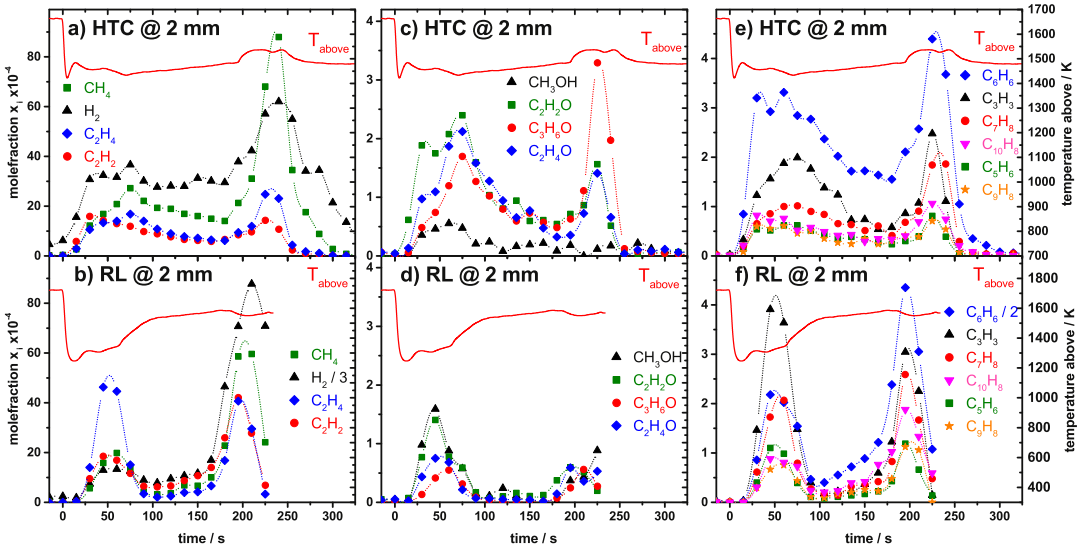

Fig. 5. Selected MBMS volatile species (symbols) and temperature profiles (red lines) from 2 mm above the analyte plate of HTC (a, c, and e) and RL (b, d, and f). All lines in the experimental data shall guide the eye and do not reflect the measurement points.

Indeed, this deceleration becomes apparent in the decreased slope of the mole fraction profile of CO and the optical observations (Fig. 3b, c). In conclusion, the phase within the first 100 s only includes volatile release and homogeneous combustion and can provide significant insights into the speciation of these processes. Once the devolatilization rate decreases sufficiently, oxygen is not fully consumed in the gas phase, it reaches the surface, and initializes char ignition. Due to char oxidation, the heat transfer through the solid is strongly enhanced and the temperature below the plate (T_{below}, Fig. 4 lower panel) rises with a significantly increased rate of 672 K/min at 200 s. This shock heat-up leads to an extremely fast release of volatiles from the remaining coal, which then react with the present oxygen. Apparently, the second devolatilization releases all remaining volatiles from the solid, since oxygen is consumed completely up to a height of 4 mm and CO shows a peak mole fraction of 36 % at 2 mm. The influence of this effect can also be observed in the time histories of CO_2 and CO shown in the middle panel of Fig. 4. For early devolatilization, the release of volatiles is slow enough to get CO oxidized to CO_2 proportionally, while during the second phase, the amount of CO and volatiles in the gas-phase close to the surface is too high to be fully oxidized. However, for 4 and 5 mm sampling height, where not all oxygen is consumed, the CO_2 mole fraction increases as a result of CO oxidation. Finally, the observed two-staged devolatilization process under these conditions takes up to 300 s, after which only the expected combustion products CO_2 and H_2O as well as excess oxygen are observed at all sampling heights.

3.2. Comparison of different coal samples

Besides other techniques commonly applied for coal volatile combustion analysis, the benefit of MBMS is its capability to measure a large number of evolving species in-situ. In the present study, a total of 49 (RL) and 47 (HTC) species were detected and quantified in the gas phase above the plate surface. Figure 5 shows a comparison of selected volatile species released by the two coals at a sampling height of 2 mm. Generally the observed trends are similar for both coals, but the double-staged effect is more sharply pronounced in RL combustion. Here, although HTC features lignite-like properties in terms of H/C and O/C ratio [15] other differences in properties, such as different specific heats, molecular structures, and textures of the coal powders used for plate molding can play a significant role. For instance, HTC has a more fiber-like network due to the hemicellulose used in the hydrothermal carbonization process, while the RL has a major share of lignin and was used as a powder with particle sizes smaller than 50 μm. Another important factor is the water content of both samples. The temperature histories shown in all panels of Fig. 5 denote that RL had a higher water content than the HTC, since the temperature drop after insertion is significantly stronger. These properties influence gas- and temperature transport through the plates, which can lead to some of the observed differences in volatile release over time, which potential models for describing the combustion of coal need to be able to describe.

Panels a and b of Fig. 5 show profiles of small volatile species like H_2, CH_4, C_2H_2, and C_2H_4 that are typically formed throughout the devolatilization process [22]. These species appear with the highest mole fractions in the order of 10^{-3} among the volatile species detected. For HTC, CH_4, with a peak mole fraction of $8.7 \cdot 10^{-3}$, is the most abundant species followed by H_2, C_2H_4, and C_2H_2, all released predominantly in the second phase governed by a much higher heating rate. A different mole fraction distribution is detected for RL. Here, the highest mole fraction of $2.6 \cdot 10^{-2}$ was found for H_2, while all other species peak with mole fractions in the same order of magnitude as in the HTC measurements. It indicates a higher content of carbon structures that can release H_2 via elimination reactions in RL, while HTC possesses more structures that contain unsaturated or oxygenated bonds. This is consistent with the results obtained from Düdder et al. [15], where the same HTC and RL samples have been analyzed with ^{13}C MAS NMR spectroscopy and a higher content of aliphatic C structures was found to be within RL than in HTC. Oxygenated species have also been detected in the experiment and are presented in Fig. 5c and d. Here, CH_3OH, C_2H_2O, C_3H_6O, and C_2H_4O have been quantified and were calibrated as methanol, ketene, acetone, and acetic acid. For these species, higher mole fractions were found for HTC, since the skeletal structure of HTC contains higher amounts of oxygen in the form of $C-O$ bonds and keto- and aldehyde functions [15]. Furthermore, these species are released slightly stronger in the first phase of devolatilization, which deduces preferably decarboxylation to happen in the HTC. However, the release of methanol was found to be stronger in RL than in HTC, which can be traced back to the removal of large numbers of functional methoxy groups from the lignin substructures. Figure 5e and f show species with a higher carbon content from C_3 up to C_{10} that were calibrated as the most probable species at the given mass, i. e. propargyl (C_3H_3), benzene (C_6H_6), cyclopentadiene (C_5H_6), toluene (C_7H_8), indene (C_9H_8), and naphthalene ($C_{10}H_8$). Information about these species are of particular interest, because they can serve as tracers for bigger tar species that are most likely already decomposed within the solid phase due to secondary pyrolysis. Overall, the evaluation shows that the mole fractions of all these species are on the same order of 10^{-4}. Additionally, a similar descending order in the peak values from $C_6H_6 > C_3H_3 > C_7H_8 > C_{10}H_8 > C_5H_6 > C_9H_8$ was found for both coals. Differences are observed in the absolute mole fractions of benzene, where RL was found to release an amount twice as high ($8.7 \cdot 10^{-4}$ vs. $4.3 \cdot 10^{-4}$) than HTC. This difference can again be attributed to the coal skeletal structure. RL, a real lignite coal, has a partly lignin skeletal structure that contains a large amount of phenolic structures, whereas HTC is produced from hemicellucosic material that predominantly contains five-membered ring structures from polysaccharides [15]. Therefore, a higher release of benzene from RL is reasonable and expected. For the other species, the maximum mole fractions seem to be less at the first peak for HTC, while being similar among both coals in the second peak. A time integration of the peak areas revealed that due to the long first devolatilization phase of the HTC, the amount produced of these species from HTC is roughly similar than for RL. In contrast to the different amounts of light volatile and oxygenated components released, no significant differences in tar composition were observed. This effect was probably due to the similarity in the rank of the two fuels, which supports the lumped modeling approach of tar species adopted for instance in the CPD model [23].

4. Conclusions

In this work, in-situ time-resolved molecluar-beam mass spectrometry was used to investigate the gas-phase speciation of oxy-fuel coal combustion in a stagnation flow configuration. This novel approach, combining an easy-to-model experimental setup and state-of-the-art measurement techniques allows to examine combustion of solid fuels with detailed speciation. For this first application, a commonly used lignite coal and a surrogate derived from hydrothermal carbonization of cellulose with similar O/C and H/C ratio were studied. Speciation data combined with temperature data and optical imaging were used to identify different phases, characteristic for the combustion of solid fuels on a macromolecular level. A two-staged devolatilization process was observed where the first stage was identified as devolatilization and homogeneous combustion and the second peak to be caused by a rapid heating of the lower regions of the coal plates leading to convolution of devolatilization, homogeneous combustion and char oxidation. Furthermore, quantification of species during the devolatilization gave insights into the connection of volatile species to the molecular structure of the coals. Finally, this study demonstrates the potential of such measurements, which can support future detailed modeling approaches of coal combustion with valuable comprehensive datasets for validation, especially by tuning e.g. gas composition and plate thickness.

Acknowledgments

The authors gratefully acknowledge financial support by the Deutsche Forschungsgemeinschaft within the framework of the collaborative research

center SFB/Transregio 129 “Oxyflame”. We additionally thank the workgroup of Prof. Dr. M. Muhler, especially A. Wütscher, for supplying us with HTC.

Supplementary material

Supplementary material associated with this article can be found, in the online version, at doi:10.1016/j.proci.2018.07.003.

List of supplemental material

One supplemental material file, including two parts, is available:

- S.I: Technical details of the Electron-ionization Time-of-flight molecular-beam mass spectrometer
- S.II: Experimental data from RL coal and peak mole fractions

References

[1] U.S. Energy Information Adminstration, https://www.eia.gov/outlooks/ieo/, accessed 15th November 2017.
[2] International Energy Agency, *20 Years of Carbon Capture and Storage*, International Energy Agency (IEA), 2016.
[3] L. Smooth, P. Smith, *Coal Combustion and Gasification*, Plenum Press, New York, NY, 1979.
[4] P. Solomon, D. Hamblen, R. Carangelo, M. Serio, G. Deshpande, *Energy Fuels* 2 (4) (1988) 405–422.
[5] J. Yu, J. Lucas, T. Wall, *Prog. Energy Combust.* 33 (2) (2007) 135–170.
[6] P.R. Solomon, M.A. Serio, E.M. Suuberg, *Prog. Energy Combust.* 18 (2) (1992) 133–220, doi:10.1016/0360-1285(92)90021-R.
[7] H. Haustein, T. Kreitzberg, B. Govert, A. Massmeyer, R. Kneer, *Fuel* 158 (Supplement C) (2015) 263–269, doi:10.1016/j.fuel.2015.05.038.
[8] S. Heuer, O. Senneca, A. Wütscher, et al., *Fuel Process. Technol.* 150 (1) (2016) 41–49.
[9] D. Dayton, R. French, T. Milne, *Energy Fuels* 9 (1995) 855–865.
[10] G. Gentile, P. Debiagi, A. Cuoci, A. Frassoldati, E. Ranzi, T. Faravelli, *Chem. Eng. J.* 321 (2017) 458–473.
[11] T. Niioka, M. Takahashi, M. Izumikawa, *Combust. Flame* 35 (1979) 81–87.
[12] W. Visser, G. Adomeit, *Symp. (Int.) Combust.* (1984) 1845–1851.
[13] N. Hansen, T. Cool, P. Westmoreland, K. Kohse-Höinghaus, *Prog. Energ. Combust.* 35 (2) (2009) 168–191. https://doi.org/10.1016/j.pecs.2008.10.001.
[14] F. Herrmann, P. Oßwald, K. Kohse-Höinghaus, *Proc. Combust. Inst.* 34 (1) (2012) 771–778.
[15] H. Düdder, A. Wütscher, R. Stoll, M. Muhler, *Fuel* 171 (2016) 54–58, doi:10.1016/j.fuel.2015.12.031.
[16] C. Morley, GasEQ Chem. Equilibria Perfect Gases, accessed 2nd November 2017, available at http://www.gaseq.co.uk/.
[17] M. Schenk, L. Leon, K. Moshammer, et al., *Combust. Flame* 160 (3) (2013) 487–503, doi:10.1016/j.combustflame.2012.10.023.
[18] P. Oßwald, H. Güldenberg, K. Kohse-Höinghaus, B. Yang, T. Yuan, F. Qi, *Combust. Flame* 158 (1) (2011) 2–15, doi:10.1016/j.combustflame.2010.06.003.
[19] C. Shaddix, Correcting thermocouple measurements for radiation loss: a critical review, *Proceedings of the Thirty Third National Heat Transfer Conference*, 1999.
[20] Y. Chen, S. Mori, W.-P. Pan, *Thermochim. Acta* 275 (1996) 149–158.
[21] D. Magalhaes, F. Kazanc, A. Ferreira, M. Rabacal, M. Costa, *Fuel* 207 (2017) 154–164.
[22] M. Serio, D. Hamblen, J. Markham, P. Solomon, *Energ. Fuels* 1 (1987) 138–152.
[23] A. Brown, T. Fletcher, *Energy Fuels* 12 (4) (1998) 745–757.